Article

Not peer-reviewed version

Influence of Single- and Double-Aging Treatments on the Mechanical and Corrosion Resistance of Alloy 625

Barbara Rivolta *, Riccardo Gerosa, Davide Panzeri

Posted Date: 21 March 2024

doi: 10.20944/preprints202403.1244.v1

Keywords: Alloy 625; Aging treatment; Mechanical strength; Corrosion resistance

 doi:10.20944/preprints202403.1244.v1

Article

Influence of Single- and Double-Aging Treatments on the Mechanical and Corrosion Resistance of Alloy 625

Barbara Rivolta *, Riccardo Gerosa and Davide Panzeri

Politecnico di Milano, Department of Mechanical Engineering, via La Masa 1, Milan, Italy
* Correspondence: barbara.rivolta@polimi.it

Abstract: The nickel-chromium-molybdenum alloy 625 exhibits an excellent combination of mechanical properties and corrosion resistance. However, the high temperature plastic deformation process and the heat treatment represent critical aspects and the adoption of non-optimal parameters can result in excessive grain coarsening and loss in mechanical strength. This detrimental behavior is worsened by the presence of a narrow region of temperatures and strain rates for complete recrystallization and the absence of phase transformation temperatures. In this alloy, the chemical composition permits slow precipitation-hardening response upon single aging. Therefore, when the soft- or solution-annealed condition is associated with insufficient mechanical properties, this potentiality can be exploited to improve the mechanical strength and prevent waste of material and resources. Since the precipitation kinetic of the hardening γ'' phase can be accelerated by prior nucleation treatment, different time-temperature combinations of double aging at 732 °C and 621 °C are investigated to reduce the overall heat treatment time. However, the simultaneous precipitation of intergranular carbides can dramatically affect the corrosion resistance. For this reason, a performance map is developed to compare all the tested conditions and identify the best compromise between the mechanical and corrosion properties.

Keywords: alloy 625; aging treatment; mechanical strength; corrosion resistance

Introduction

The nickel-chromium-molybdenum-niobium Alloy 625, patented in 1964 by H. L. Eiselstein and J. Gadbut, provides excellent mechanical and corrosion properties thanks to the presence of high amounts of chromium, molybdenum and niobium [1–11]. The excellent potentialities of this material are mainly exploited for applications in the oil and gas and automotive fields [1,4,6,11]. The ASTM B446 standard [12] reports two possible heat treating conditions for this material: soft annealing and solution annealing. For applications below 600 °C where good combination of tensile strength and corrosion resistance is required, soft annealing is recommended, and it requires a minimum temperature of 871 °C [12]. The solution-annealing treatment is suggested for high creep strength, and it is performed at a minimum of 1093 °C for applications above 600 °C [12]. In the soft-annealed condition, this alloy shows a fully austenitic microstructure with a heterogeneous distribution of primary carbides and nitrides which are induced by the solidification process [8–11,13]. These compounds are mainly enriched in niobium and titanium, which are depleted from the surrounding regions. The process- and service-induced thermal exposure above 600 °C can activate complex precipitation phenomena that can significantly alter both the mechanical properties and the corrosion resistance [1,10]. However, the formation of hardening phases can be exploited to recover insufficient mechanical properties in the solution- or soft-annealed condition [12]. The time-temperature-precipitation (TTP) diagram of this alloy is shown in Figure 1 [10]. The precipitate phases reported in the literature for this alloy are MC, M_6C and $M_{23}C_6$ metal carbides, intermetallic phases, normally γ'', δ and Laves [10,14,15]. The precipitation of intergranular carbides and intermetallic phases induces sensitization, reduction of toughness and deformability. The susceptibility to intergranular corrosion

 doi:10.20944/preprints202403.1244.v1

is increased by the formation of intergranular carbides rich in chromium and molybdenum. In fact, these alloying elements are depleted from the surrounding regions preventing the auto-passivation mechanism [1–4,10,16–18]. Moreover, intergranular cracking is favoured by the formation of intergranular films of carbides resulting in a reduction of toughness. In this material, the presence of insufficient mechanical properties is a common issue, and it is related to the difficulty in retaining a fine-grained structure during processing and heat treatment. In fact, regarding the high-temperature plastic deformation process, the optimal region of temperatures and strain rates is very restricted. For this reason, the plastic deformation procedure should be carefully designed, but very often, depending on the available equipment and the component geometry, the recrystallization process is not optimal. Moreover, grain refinement via heat treatment cannot be obtained because of the absence of phase transformation temperatures. Furthermore, these detrimental characteristics are worsened by the fact that both the soft- and the solution-annealing treatments are inevitably associated with grain coarsening which degrades the overall mechanical performance [11,19,20]. Therefore, because the mechanical properties are directly related to the grain size [11], the heat treatment parameters should be tuned as to provide the best compromise between the solubilization level, which affects the corrosion resistance, and the grain size, which determines the mechanical strength. The possibility to recover the strength loss induced by excessive grain coarsening by aging treatment is very useful, but this requires a careful optimization to find the best balance between the mechanical and corrosion properties and the heat treatment time, which directly affects costs and energy consumption. The ordered intermetallic γ'', Ni_3Nb, hardening phase is obtained upon aging from 600 °C to 800 °C [10,14,21]. In the literature, Moore et al. and Suave et al. [1,20,22] investigated the single-aging response in temperature range from 600 °C to 800 °C and from 550 °C to 900 °C, respectively. However, the hardening effect was significant only after very long exposures, which are typically not compatible for industrial applications. This strength improvement is generally obtained at the expense of deformability and corrosion resistance which is worsened by the precipitation of Cr-rich carbides. This research paper investigates nonstandard double-aging treatments to recover insufficient mechanical properties in the soft-annealed condition and it represents a development of our previous published work about this topic (Rivolta et al. [23]). This additional investigation is fundamental to obtain a more accurate definition and optimization of the aging treatment based on the service and standard requirements. Such investigation was anticipated by a preliminary analysis of the single-aging response at 732 °C and 621°C. Regarding the aging treatment of Alloy 625, Eiselstein and Tillack [7] identified that a minimum aging time from 730 °C to 840 °C is needed to markedly accelerate the γ''-induced hardening effect at 650 °C. This multistage aging treatment was called "nucleation treatment and aging". The strength improvement allowed by single- and double-aging treatments can be exploited to reduce the consumption of resources and the carbon footprint thanks to the thickness and mass reduction. Moreover, the reduction of the component weight enables lower fuel consumption and operative costs.

The adoption of dilatometric techniques to study the kinetics of nucleation, coalescence, growth and dissolution of precipitates is widely present in the literature [23–25]. Therefore, also for this material, the microstructural changes upon single- and double-aging treatments can be investigated using dilatometric tests to detect and analyse the effects of phase precipitation and transformation. For instance, Pasiowiec et al. [25] adopted continuous heating and isothermal dilatometric tests to investigate and compare the precipitation kinetics of the wrought and the laser powder bed fused Alloy 625. The variations in the thermal expansion coefficient were more pronounced in the laser powder bed fused Alloy 625 because of the accelerated kinetics of γ'' precipitation. Such dilatometric analyses will be performed in a future work.

In this work, the aging treatment is studied by hardness, tensile and corrosion tests for both single and double aging with different time-temperature combinations. Its investigation was developed starting from the double aging recommended for alloy CarTech® Custom Age 625 PLUS® [26,27]. In this case, compared to the conventional alloy 625, a higher titanium content is present to promote the formation of γ'' Ni_3Nb precipitates [14,26,27]. Regarding this variant, the best combination of age-hardening response and corrosion resistance is obtained with double aging at 732

 doi:10.20944/preprints202403.1244.v1

°C for 8 h and 621 °C for 8 h after soft-annealing treatment at 1038 °C [26,27]. The resistance to intergranular corrosion was analysed in selected aging conditions according to the ASTM G28-A standard [28]. The corrosion rate limit was considered equal to 1.20 mm/year. The experimental results of this research work are finally reported in a performance map to provide a graphical and more effective overview of the relationship between the mechanical properties and the corrosion resistance upon aging treatment.

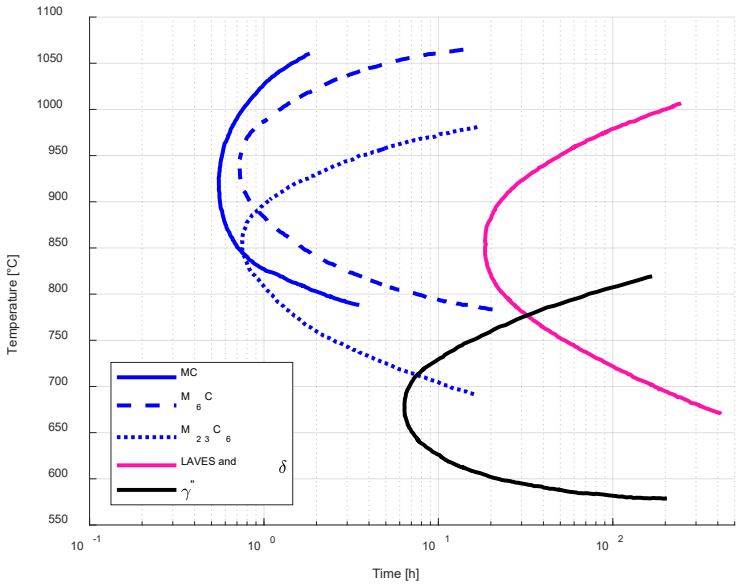

Figure 1. Experimental Time-Temperature-Precipitation (TTP) diagram of Alloy 625. Adapted from [10,29].

2. Materials and Method

The material investigated in this work is a forged and untreated Alloy 625 rod with diameter of 60 mm. Heat treatments were carried out in a laboratory furnace. The tensile specimens were machined in the longitudinal direction. Samples for the microstructural analyses and the hardness tests were prepared according to the conventional metallographic procedure. After grinding and polishing, etching was carried out in five parts HCl diluted in one part 30 % H_2O_2 for 10 s [5,26,30]. Microstructural analyses were performed using a Leica (model DMR) light optical microscope and a Zeiss (model SIGMA 500) scanning electron microscope. The HV30 Vickers hardness tests were conducted using a Wolpert Testor 930 hardness tester in accordance with the EN ISO 6507 standard [31]. In each tested condition, at least five hardness measurements were carried out. Tensile tests were performed using round proportional specimens tested with an INSTRON model 4507 machine, according to the EN ISO 6892 standard [32]. The intergranular corrosion tests were carried out in a solution of ferric sulfate, $Fe_2(SO_4)_3$ and sulphuric acid, H_2SO_4 for 120 h, in accordance with the ASTM G28 – Method A standard [28]. The mechanical strength requirements considered for the evaluation of acceptability were taken from the ASTM B446 standard [12]. For the corrosion resistance, a maximum corrosion rate of 1.20 mm/year was considered. SEM and chemical EDXS analyses were carried out to better investigate the relationship between the microstructural constituents and the corrosion properties. The qualitative EDXS chemical analyses were performed using the OXFORD Altee Energy – Advanced detector. The bulk chemical composition was investigated by OES spectroscopy. The results are reported in Table 1. Based on the requirements of the ASTM B446 standard [12], the chemical composition is acceptable.

Table 1. Chemical composition by OES spectroscopy of material investigated in this paper.

	Ni	Cr	Mo	Nb	Fe	Mn	Ti	Al	C	Si	P	S
wt. %	62.3	20.4	8.50	3.59	4.41	0.09	0.30	0.20	0.04	0.17	<0.01	<0.01

 doi:10.20944/preprints202403.1244.v1

Before the aging treatment, all the samples and specimens were soft annealed at 1038 °C for 0.5 h and water quenched. The hardening response upon isothermal single-aging treatments was investigated at 732 °C and 621 °C. After this preliminary analysis, double-aging treatments were carried out changing the exposure times at both the primary aging temperature (732 °C) and the secondary aging one (621 °C). Hardness tests were performed in each aging condition investigated in this work. Successively, based on the hardness results, tensile and corrosion tests were carried out in a selection of aging conditions. SEM and EDXS analyses were performed to investigate the relationship between the microstructural constituents and the corrosion properties.

3. Results and Discussion

The as-forged material was soft-annealed at 1038 °C for 0.5 h in accordance with the ASTM B446-19 standard [12]. The microstructural investigation was performed by metallographic analysis using light-optical and scanning-electron microscopy. As reported in Figure 2, the austenitic microstructure showed presence of equiaxed and twinned grains without intergranular carbides. The average grain size measured according to the ASTM E112 standard was equal to 65 μm [33].

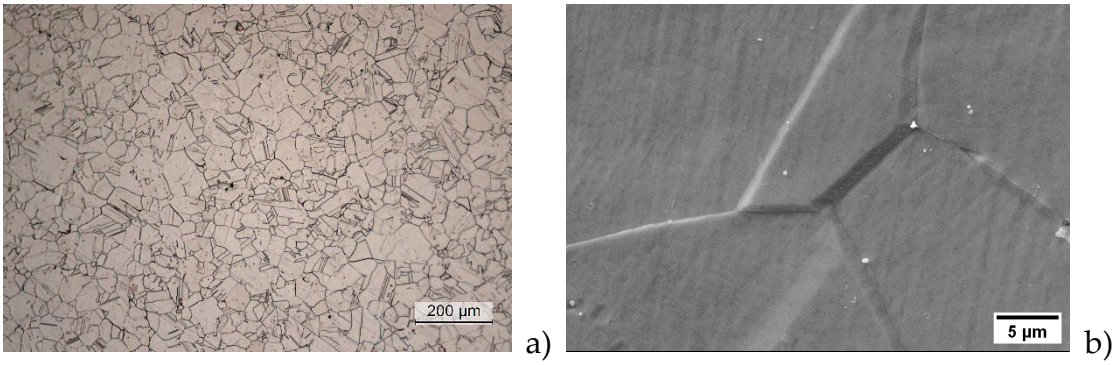

Figure 2. Soft-annealed condition at LOM and SEM. a) Light-optical micrograph showing presence of equiaxed and twinned austenite grains; b) Scanning-electron micrograph showing absence of intergranular carbides.

Then, the soft-annealed material was characterized by room-temperature tensile and hardness tests. The mechanical properties are reported in Table 2. The mechanical strength in the soft-annealed condition is not compatible with the minimum yield strength requirement (414 MPa) [12].

Table 2. Mechanical properties of the soft-annealed material determined by hardness and tensile tests at room temperature.

	Hardness	Yield strength [MPa]	Ultimate Tensile Strength [MPa]	A%	Z%
This work	194 HV30	350	829	61.0	70
ASTM B446	---	>414	>827	>30.0	---

In the soft-annealed condition, the presence of a corrosion rate equal to 0.65 mm/year confirms the suitability of this heat treatment (1038 °C 0.5 h).

After soft-annealing at 1038 °C for 0.5 h, the age-hardening effect was investigated with isothermal single-aging treatments at both 732 °C and 621 °C up to 600 h starting from the results of a reduced set of conditions studied in our previous work [29]. The overall set of hardness data at both aging temperatures is reported in Figure 3 [29]. As shown in Figure 3, upon single aging at 621 °C, a steep hardness increase is obtained starting from 72 hours. Until such exposure, the hardness increment with respect to the soft-annealed condition is less than 10 %. At 732 °C, the precipitation hardening effect is slightly higher compared to that at 621 °C at least until the exposures tested in this work. At 621 °C, a satisfying hardening effect is obtained only after very long exposures and this behavior can limit its exploitation for most industrial applications. Such very slow age-hardening

 doi:10.20944/preprints202403.1244.v1

kinetic is also confirmed by the literature data of Moore et al. and Suave et al. about single aging from 550 °C to 900 °C [1,20,22]. The hardness values of our work are compatible with the literature [20]. The age-hardening phenomenon in this temperature range is determined by precipitation of the γ'' phase, as shown in the TTP curves of Figure 1. According to the TTP curves, at these aging temperatures, the formation of intergranular $M_{23}C_6$ carbides can occur together with the intermetallic hardening γ'' precipitates. However, compared to the γ'' phase, the hardening effect of the $M_{23}C_6$ carbides is negligible [15]. The simultaneous formation of Cr-rich $M_{23}C_6$ carbides was deeply investigated by EDXS analyses performed by scanning electron microscopy. The IDs of the tested positions are reported in Figure 4 and the results of the EDXS analyses are given in Table 3. As shown in Table 3 and Figure 4, at 732 °C, intergranular Cr-rich carbides were not present until 1 hour and the onset of their formation was detected in the 3 hours sample. According to the EDXS analyses reported in Table 3, the intergranular carbides observed in the samples aged at 732 °C were mainly enriched in chromium, as confirmed by the literature data [10,14]. The formation of such carbides is expected to be significantly detrimental to the corrosion resistance.

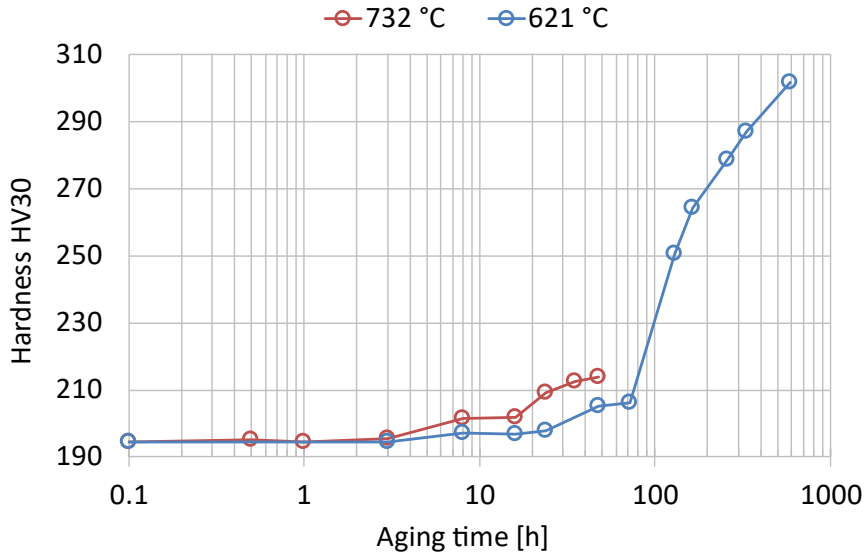

Figure 3. Hardness curves of the soft-annealed alloy 625 after single-aging treatments.

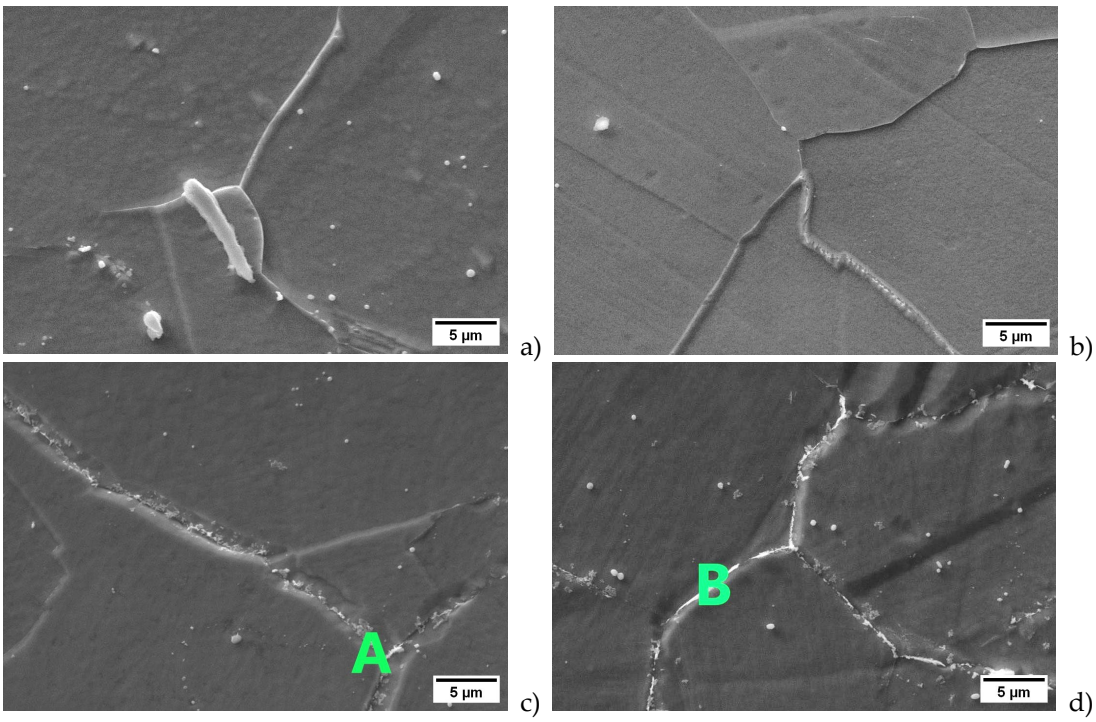

 doi:10.20944/preprints202403.1244.v1

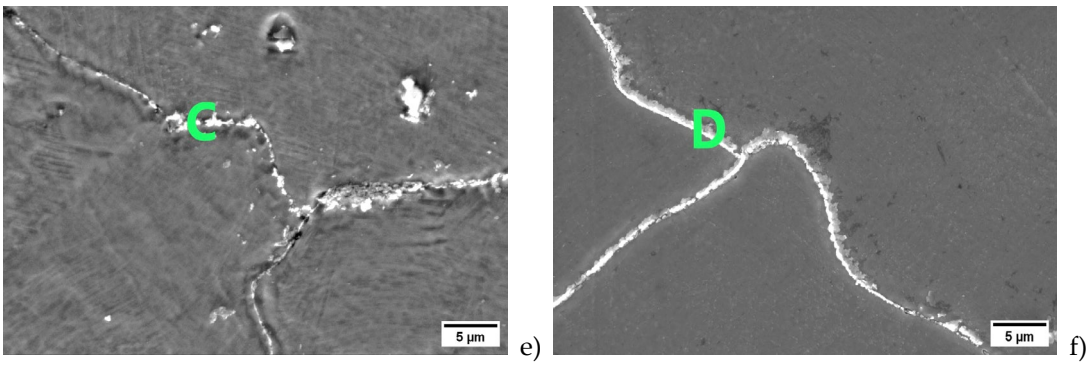

Figure 4. SEM micrographs of the samples aged at 732 °C for different times: **a**) 732 °C 0.5 h; **b**) 732 °C 1 h; **c**) 732 °C 3 h; **d**) 732 °C 8 h; **e**) 732 °C 24 h; **f**) 732 °C 48 h.

Table 3. EDXS analyses in wt. % at the positions reported in Figure 4.

	ID	Ni	Cr	Mo	Nb	Fe	Ti	Al	Si
OES analysis	---	62.3	20.4	8.50	3.59	4.41	0.30	0.20	0.17
Figure 4.c	A	61.1	23.7	7.00	3.02	4.31	0.36	0.37	0.14
Figure 4.d	B	54.4	25.2	10.40	4.53	4.03	0.58	0.51	0.35
Figure 4.e	C	52.8	29.5	9.77	2.96	4.13	0.29	0.30	0.25
Figure 4.f	D	52.1	30.3	8.75	4.22	3.89	0.37	0.17	0.20

At 621 °C, the precipitation of the hardening γ'' phase is faster than that of the intergranular Cr-rich carbides. In fact, according to the TTP diagram of Figure 1, at this temperature, the formation of $M_{23}C_6$ carbides requires longer exposures compared to 732 °C. This difference was confirmed by the SEM and EDXS analyses performed on the samples aged at 621 °C. The results are reported in Figure 5 and Table 4. In this work, Cr-rich carbides were observed at the grain boundaries of the sample aged at 621 °C for 592 h, and they were not detected on shorter exposures. So, upon aging at 621 °C, it is possible to exploit the precipitation of the hardening intermetallic γ'' phase before worsening the corrosion resistance.

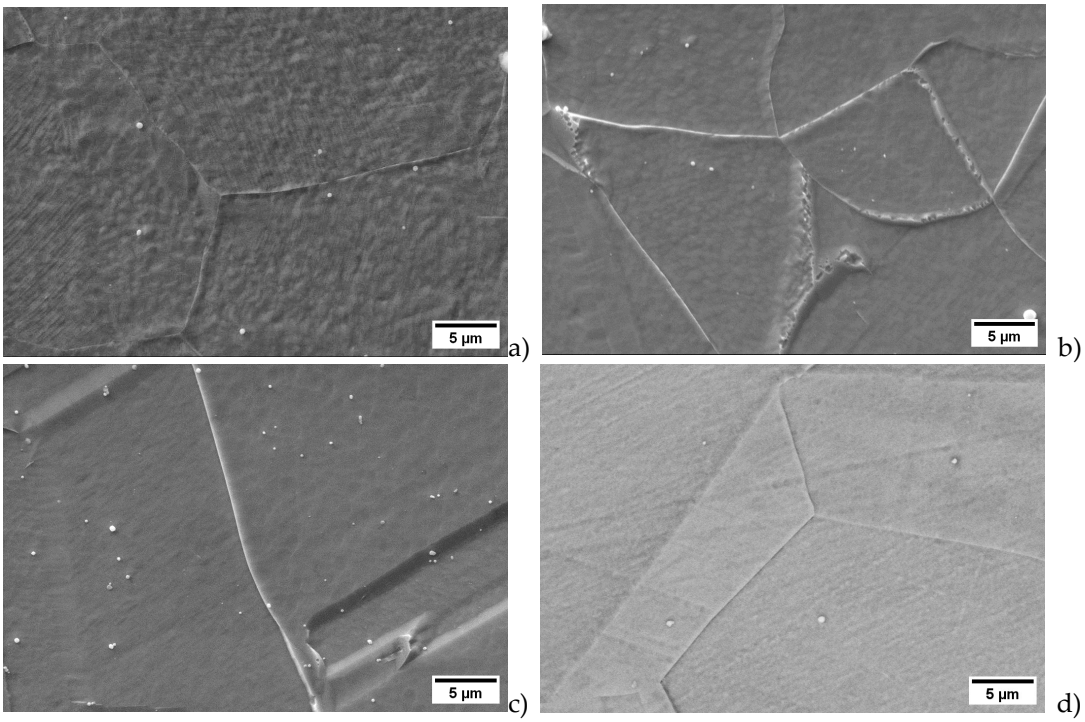

 doi:10.20944/preprints202403.1244.v1

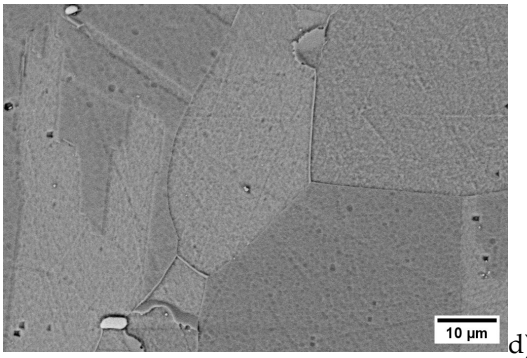

d)
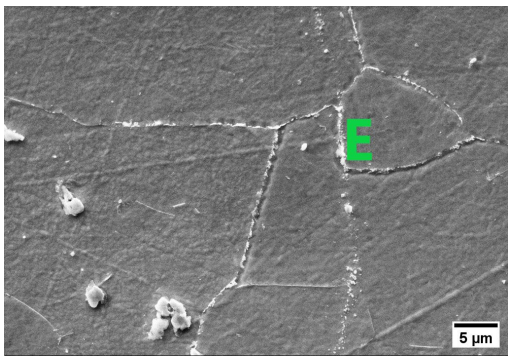

e)

Figure 5. SEM micrographs of the samples aged at 621 °C for different times: **a**) 621 °C 16 h; **b**) 621 °C 48 h; **c**) 621 °C 130 h; **d**) 621 °C 165 h; **e**) 621 °C 260 h; **f**) 621 °C 592 h.

Table 4. EDXS analyses in wt. % at the positions reported in Figure 5.

	ID	Ni	Cr	Mo	Nb	Fe	Ti	Al	Si
OES analysis	---	62.3	20.4	8.50	3.59	4.41	0.30	0.20	0.17
Figure 5.e	A	59.6	23.81	8.41	2.71	4.51	0.31	0.42	0.23

After the investigation of single-aging response, the possibility of accelerating the precipitation kinetic by double-aging treatments was studied considering different time-temperature conditions with primary aging at 732 °C (up to 48 h) and secondary aging at 621 °C (up to 592 h). Double-aging treatments significantly accelerate the γ'' precipitation. In fact, fixing the duration of the secondary aging, the precipitation kinetic is accelerated increasing the prior exposure at 732 °C. In this case, short primary aging times are sufficient to obtain the peak hardness. The adoption of longer primary aging time is not associated with a further improvement in the mechanical strength. In fact, when the peak hardness is reached, the hardness curve remains almost flat. Considering the TTP diagram reported in Figure 1, the major drawback of such double-aging procedure is represented by the primary aging temperature. In fact, even though the primary aging enables significant acceleration of the γ'' formation, such aging temperature is also associated with a faster precipitation of intergranular carbides which are extremely detrimental to the corrosion resistance. For this reason, it is required to limit as much as possible the primary aging exposure. Regarding the double aging, Eiselstein and Tillack [7] found an increase of hardness from 170 HV to 210 HV adopting a primary treatment at 760 °C for 1 h prior to aging at 621 °C for 72 h. In our research work, the hardness increases from 195 HV to 280 HV with double aging at 732 °C for 1 h and 621 °C for 72 h. As described in the Introduction, this double-aging procedure was investigated starting from that of the alloy CarTech® Custom Age 625 PLUS® [26,27] for which the suggested double-aging treatment resulted in a hardness increase from 188 HV to 353 HV. Regarding our research work, the same heat treatment was associated with a poorer hardening response (from 194 HV to 220 HV) because of the lower titanium content.

Successively, in selected double-aging conditions, room-temperature tensile tests were performed. As shown in Figure 7, the tensile properties show a trend similar to that observed for the hardness curves reported in Figure 6. In fact, after a certain exposure, the increase in the primary aging time with fixed secondary aging does not provide any further improvement for both the yield strength and the ultimate tensile strength. The hardening effect obtained by double aging is obtained at the expense of tensile deformability. In fact, a reduction of both A% and Z% was observed. However, the A% values remained well above the minimum standard requirement (30 %) [12]. In all the tested double-aging conditions, except 732 °C 3 h plus 621 °C 8 h, both the yield strength and the ultimate tensile strength were compatible with the minimum standard requirements [12]. Therefore, when insufficient tensile properties characterize the soft- or solution-annealed condition, this aging procedure can be exploited to obtain satisfying strength improvements with reasonable heat treatment times compared to single aging. In fact, as previously described, compared to single-aging treatments, the double aging allows to significantly accelerate the hardening kinetic. As reported in

 doi:10.20944/preprints202403.1244.v1

Table 5, with double aging at 732 °C 3 h and 621 °C 72 h, it is possible to obtain the same mechanical properties of single aging at 621 °C for 260 h with a conspicuous acceleration of the aging response and consequent reduction of the heat treatment time and cost.

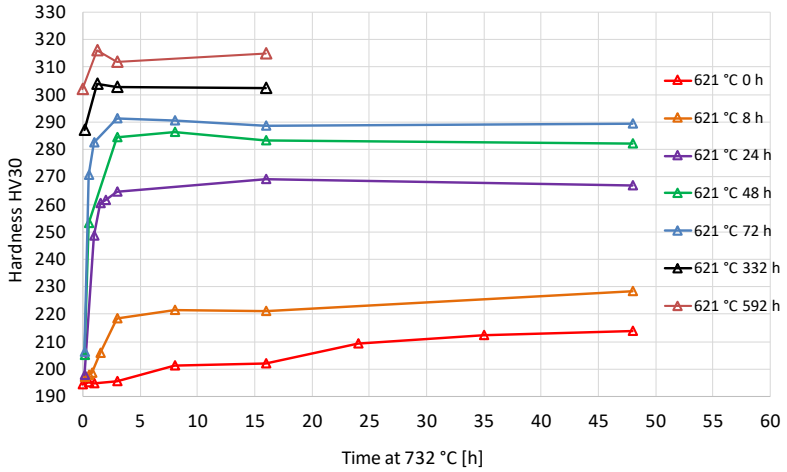

Figure 6. Double aging Vickers hardness curves of the forged and soft-annealed alloy 625 with different combinations of double-aging times at 732 °C and 621 °C.

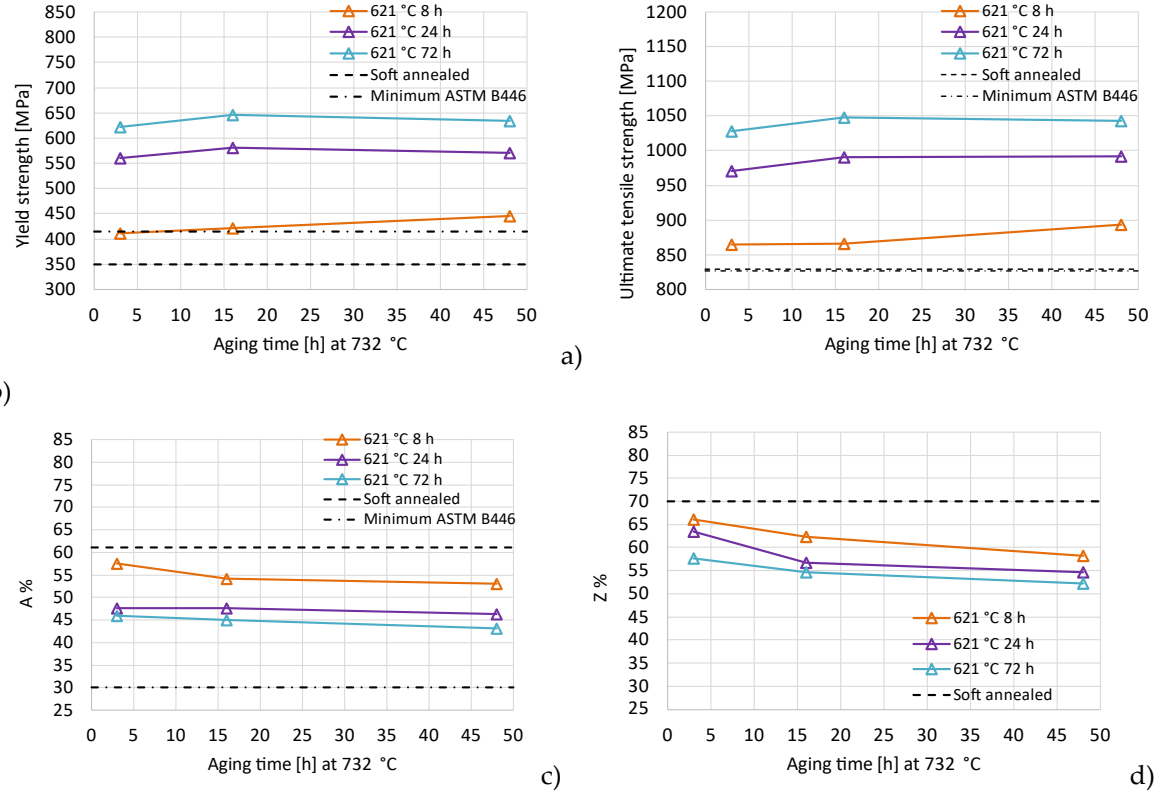

Figure 7. Room-temperature tensile properties in different double-aging conditions: **a**) Rp0.2; **b**) UTS; **c**) A%; **d**) Z%.

Table 5. Comparison of the tensile properties upon single- and double-aging treatments with respect to the soft-annealed condition.

Condition	Hardness HV30	Yield Strength [MPa]	Ultimate Tensile Strength [MPa]	A%	Z%
Soft-annealed (SA)	194	350	829	61.0	70

 doi:10.20944/preprints202403.1244.v1

SA + 621 °C 260 h	279	604	1039	46.0	62
SA + 732 °C 3 h + 621 °C 72 h	280	616	1023	47.0	57

The possibility of estimating the tensile properties from the results of hardness tests represents a fast and useful tool in the analysis and comparison of different time-temperature aging conditions. The relationship between the hardness and the tensile strength was investigated by regression analysis of a dataset obtained combining the results reported in this work with those previously published in the literature [11,29]. The linear regression analysis of this larger set of experimental data is reported in Figure 8 together with the determination coefficient R^2 which was adopted to assess the goodness of fit. Considering the results of this analysis and the requirements of the ASTM B446 standard [12], 192 HV and 202 HV represent the minimum hardness values for acceptable ultimate tensile strength and yield strength, respectively.

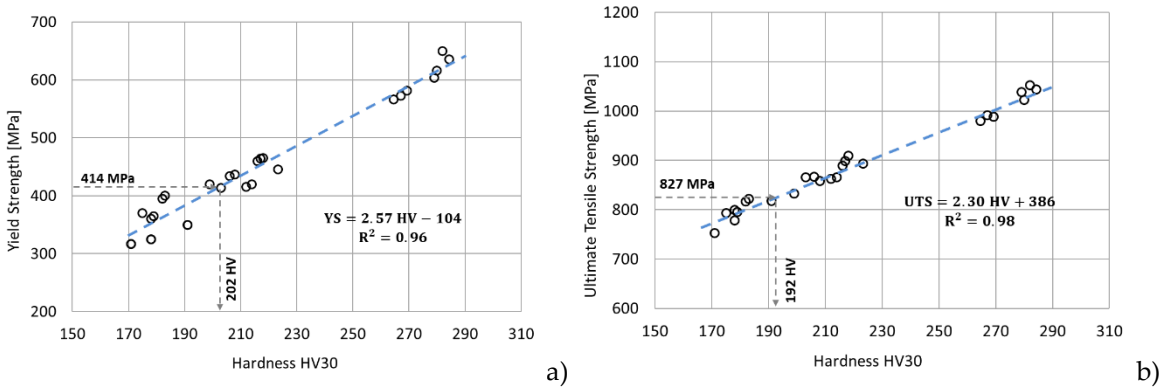

Figure 8. Relationship between the hardness and the tensile properties. Dataset obtained with the results of this research work and those previously published in the literature [11,29].

The intergranular corrosion resistance [28] was analysed in a selection of the conditions investigated in this work. The variation of the corrosion rate as function of the aging time is depicted in Figure 9 for both single and double aging. The single-aging treatment at 732 °C shows a rapid increment in the corrosion rate starting from 3 hours and, until this exposure, the hardening effect is very poor. This experimental result is confirmed by the SEM and EDXS analyses reported in Figure 4 and Table 3. In fact, single aging at 732 °C for 3 hours represents the onset of intergranular Cr-rich carbides formation which is extremely detrimental to the corrosion resistance. The rapid increase in the corrosion rate at longer exposures is associated with a more copious formation of such carbides at the grain boundaries. At 732 °C, such undesired precipitation phenomenon occurs very quickly and the reduction in corrosion resistance becomes critical much earlier than the onset of γ'' precipitation, which represents the primary hardening phase. In fact, as confirmed by the experimental results and the literature [15], the hardening effect of the intergranular carbides is very poor and the effect of sensitization is predominant. At 621 °C, the precipitation of intergranular $M_{23}C_6$ carbides is obtained only after very long exposures. This peculiarity allows to exploit the hardening effect of the γ'' precipitates without worsening the corrosion resistance. Based on the experimental results reported in Figure 9, at 621 °C, the rapid increment in the corrosion rate is no longer obtained from 3 hours, as occurs at 732 °C, but only after 130 hours. Therefore, in this case, it is possible to exploit the hardening effect reported by the hardness curves in Figure 3 before worsening the intergranular corrosion resistance. This experimental result is confirmed by the SEM and EDXS analyses reported in Figure 5 and Table 4. Regarding the double aging, the corrosion tests were performed in selected conditions to evaluate the effect of an increasing primary exposure at 732 °C with fixed secondary aging time. As shown in Figure 9, increasing the time at 732 °C, the corrosion resistance is quickly reduced because of a very rapid and copious precipitation of intergranular carbides. As shown by the results of the corrosion tests, the thermal exposure at 732 °C is surely the most critical and it should be restricted as much as possible to maintain the corrosion resistance within acceptable limits, but provide sufficient acceleration of the precipitation response. Therefore,

 doi:10.20944/preprints202403.1244.v1

in the presence of double aging, the limitation of the primary aging time is extremely important also considering that above a certain duration there is no further strength improvement.

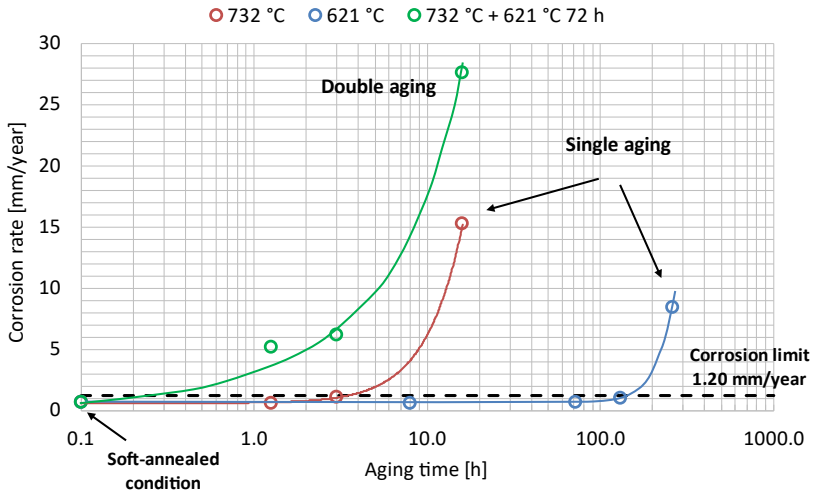

Figure 9. Corrosion rates obtained by intergranular corrosion tests (ASTM G28-A standard [28]) on different single- and double-aging conditions. Regarding the double aging curve (732 °C + 621 °C 72 h, the aging time on the horizontal axis represents the primary aging time at 732 °C.

Considering the corrosion rate limit (1.20 mm/year) and the minimum requirement for the mechanical strength (202 HV), a performance map was built with the experimental conditions tested by hardness and corrosion tests in this work and in our previous paper [29], as shown in Figure 10. The hardness limit of 202 HV was calculated considering the minimum standard requirement for the mechanical strength [12] and the relationship between the hardness and the yield strength reported in Figure 8.a. In the soft-annealed condition, only the corrosion resistance is acceptable. Single aging at 621 °C for 130 h provides good corrosion resistance and excellent mechanical strength. Longer aging times at 621 °C allow further strength improvement at the expense of a dramatic loss in the corrosion resistance. Regarding the double aging, even reducing the primary aging time down to 1 hour, the corrosion rates remain above the threshold limit. In this case, a reduction of both the primary and secondary aging times is still not sufficient to obtain acceptable corrosion resistance. Moreover, further limitation of the primary aging exposure would be not feasible in the presence of large components.

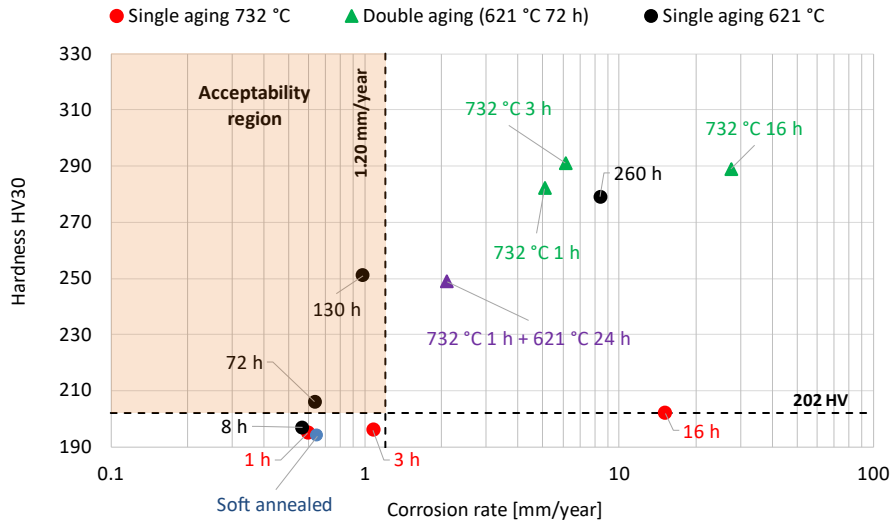

Figure 10. Experimental conditions of single and double aging tested in this work and in our previous paper [29]. The conditions positioned in the upper left quadrant with orange shading are acceptable based on the requirements for both the mechanical strength and the corrosion resistance.

 doi:10.20944/preprints202403.1244.v1

Conclusions

Single- and double-aging treatments can be adopted to improve the mechanical strength of Alloy 265, especially when the soft-annealed condition is associated with insufficient mechanical properties. However, simultaneous formation of the hardening γ'' phase and intergranular Cr-rich carbides can detrimentally affect the corrosion resistance. Such undesired phenomenon occurs very quickly at 732 °C, but it is obtained only after very long exposures at 621 °C. Therefore, at 621 °C, this behavior allows to exploit the formation of the hardening γ'' phase before obtaining the precipitation of intergranular carbides. For this reason, single aging at 621 °C for 72 h and 130 h are both acceptable. With double aging, the γ'' formation is significantly accelerated thanks to the triggering effect of the primary aging treatment. Therefore, the adoption of such prior nucleation treatment allows to appreciably decrease the heat treatment time compared to single aging at 621 °C. For instance, with double aging at 732 °C 1 h and 621 °C 24 h, it is possible to obtain the same mechanical properties of single aging at 621 °C for 130 h with a conspicuous acceleration of the aging response and consequent reduction of the heat treatment time and costs. However, the corrosion resistance is critical in the case of double aging, especially because of the primary step. In this case, even after optimization of the primary aging time, none of the tested conditions was compatible with the imposed requirements. In addition, very short aging times can be not feasible in the presence of large components.

Author Contributions: Conceptualization, B. R., R. G. and D. P.; Methodology, R. G. and D. P.; Formal Analysis, R. G. and D. P.; Investigation, B. R., R. G. and D. P.; Writing—Original Draft Preparation, D. P.; Writing—Review and Editing, B. R., R. G. and D. P.; Supervision, B. R. and R. G. All authors have read and agreed to the published version of the manuscript.

Funding: This research received no external funding.

Data Availability Statement: The raw data supporting the conclusions of this article will be made available by the authors on request.

Conflicts of Interest: The authors declare no conflict of interest.

References

1. L.M. Suave, J. Cormier, P. Villechaise, A. Soula, Z. Hervier, D. Bertheau, J. Laigo, Microstructural Evolutions During Thermal Aging of Alloy 625: Impact of Temperature and Forming Process, Metallurgical and Materials Transactions A 45 (2014) 2963–2982. https://doi.org/10.1007/s11661-014-2256-7.
2. V. Shankar, K. Bhanu Sankara Rao, S.L. Mannan, Microstructure and mechanical properties of Inconel 625 superalloy, Journal of Nuclear Materials 288 (2001) 222–232. https://doi.org/10.1016/S0022-3115(00)00723-6.
3. A. Sukumaran, R.K. Gupta, V. Anil Kumar, Effect of Heat Treatment Parameters on the Microstructure and Properties of Inconel-625 Superalloy, J Mater Eng Perform 26 (2017) 3048–3057. https://doi.org/10.1007/s11665-017-2774-8.
4. U. Heubner, J. Kloewer, H. Alves, R. Behrens, C. Schindler, V. Wahl, M. Wolf, Nickel Alloys and High-Alloyed Special Stainless Steels: Properties-Manufacturing-Applications, 4th ed., Expert-Verlag, Renningen, 2012.
5. ASM International, ASM Specialty Handbook: Nickel, Cobalt, and Their Alloys, Materials Park, 2000.
6. M.J. Donachie, S.J. Donachie, Superalloys: A Technical Guide, 2nd ed., ASM International, Materials Park, 2002.
7. H.L. Eiselstein, D.J. Tillack, The Invention and Definition of Alloy 625, in: E.A. Loria (Ed.), Proceedings on Superalloys 718, 625, and Derivatives, The Minerals, Metals & Materials Society, 1991: pp. 1–14.
8. M. Durand-Charre, The Microstructure of Superalloys, 1st ed., Routledge, London, 1968.
9. S.J. Patel, G.D. Smith, The Role of Niobium in Wrought Precipitation-Hardened Nickel-Base Alloys, in: E.A. Loria (Ed.), Proceedings on Superalloys 718, 625, 706 and Derivatives, The Minerals, Metals & Materials Society, 2005: pp. 135–154.
10. S. Floreen, G.E. Fuchs, W.J. Yang, The Metallurgy of Alloy 625, in: Superalloys 718, 625, 706 and Derivatives, The Minerals, Metals & Materials Society, 1994: pp. 13–37.
11. B. Rivolta, M.V. Boniardi, R. Gerosa, A. Casaroli, D. Panzeri, L.H. Pizetta Zordão, Alloy 625 Forgings: Thermo-Metallurgical Model of Solution-Annealing Treatment, J Mater Eng Perform (2022). https://doi.org/10.1007/s11665-022-07524-7.

12. ASTM International, ASTM B446-19: Standard Specification for Nickel-Chromium-Molybdenum-Columbium Alloy (UNS N06625), Nickel-Chromium-Molybdenum-Silicon Alloy (UNS N06219), and Nickel-Chromium-Molybdenum-Tungsten Alloy (UNS N06650) Rod and Bar, (2019).
13. R.C. Reed, C.M.F. Rae, Physical Metallurgy of the Nickel-Based Superalloys, in: Physical Metallurgy, Elsevier, 2014: pp. 2215–2290. https://doi.org/10.1016/B978-0-444-53770-6.00022-8.
14. L.-J. Yu, E.A. Marquis, Precipitation behavior of Alloy 625 and Alloy 625 plus, J Alloys Compd 811 (2019) 151916. https://doi.org/10.1016/j.jallcom.2019.151916.
15. X. Liu, J. Fan, P. Zhang, K. Cao, Z. Wang, F. Chen, D. Liu, B. Tang, H. Kou, J. Li, Influence of heat treatment on Inconel 625 superalloy sheet: carbides, γ'', δ phase precipitation and tensile deformation behavior, J Alloys Compd 930 (2023) 167522. https://doi.org/10.1016/j.jallcom.2022.167522.
16. C. Vernot-Loier, F. Cortial, Influence of Heat Treatments on Microstructure, Mechanical Properties and Corrosion Behaviour of Alloy 625 Forged Rod, in: E.A. Loria (Ed.), Proceedings on Superalloys 718, 625, and Derivatives, The Minerals, Metals & Materials Society, 1991: pp. 409–422.
17. U. Heubner, M. Köhler, Effect of Carbon Content and Other Variables on Yield Strength, Ductility, and Creep Properties of Alloy 625, in: E.A. Loria (Ed.), Proceedings on Superalloys 718, 625, 706 and Derivatives, The Minerals, Metals & Materials Society, 1994: pp. 479–488.
18. U. Heubner, M. Köhler, The effect of final heat treatment and chemical composition on sensitization, strength and thermal stability of alloy 625, in: Superalloys 718, 625, 706 and Derivatives, 1997: pp. 795–803.
19. M. Liu, W. Zheng, J. Xiang, Z. Song, E. Pu, H. Feng, Grain Growth Behavior of Inconel 625 Superalloy, Journal of Iron and Steel Research International 23 (2016) 1111–1118. https://doi.org/10.1016/S1006-706X(16)30164-9.
20. I.J. Moore, J.I. Taylor, M.W. Tracy, M.G. Burke, E.J. Palmiere, Grain coarsening behaviour of solution annealed Alloy 625 between 600–800 °C, Materials Science and Engineering: A 682 (2017) 402–409. https://doi.org/10.1016/j.msea.2016.11.060.
21. C.O. Yenusah, Y. Ji, Y. Liu, T.W. Stone, M.F. Horstemeyer, L.-Q. Chen, L. Chen, Three-dimensional Phase-field simulation of γ" precipitation kinetics in Inconel 625 during heat treatment, Comput Mater Sci 187 (2021) 110123. https://doi.org/10.1016/j.commatsci.2020.110123.
22. L.M. Suave, D. Bertheau, J. Cormier, P. Villechaise, A. Soula, Z. Hervier, J. Laigo, Impact of microstructural evolutions during thermal aging of Alloy 625 on its monotonic mechanical properties, MATEC Web of Conferences 14 (2014) 21001. https://doi.org/10.1051/matecconf/20141421001.
23. B. Rivolta, R. Gerosa, On the non-isothermal precipitation of copper-rich phase in 17-4 PH stainless steel using dilatometric techniques, J Therm Anal Calorim 102 (2010) 857–862. https://doi.org/10.1007/s10973-010-0882-x.
24. B. Rivolta, R. Gerosa, F. Tavasci, The dilatometric technique for studying sigma phase precipitation kinetics in F55 steel grade, J Therm Anal Calorim 132 (2018) 869–877. https://doi.org/10.1007/s10973-017-6940-x.
25. H. Pasiowiec, B. Dubiel, R. Dziurka, P. Bała, P. Ledwig, M. Wróbel, M. Gajewska, W. Ziaja, M. Poręba, Effect of creep deformation on the microstructure evolution of Inconel 625 nickel-based superalloy additively manufactured by laser powder bed fusion, Materials Science and Engineering: A 887 (2023) 145742. https://doi.org/10.1016/j.msea.2023.145742.
26. Carpenter Technology corporation, CarTech® Custom Age 625 PLUS® alloy: technical datasheet, (2020). www.carpentertechnology.com/alloy-finder/ 625-Plus (accessed August 25, 2020).
27. N.B. Schmidt, T.A. DeBold, R.B. Frank, Custom age 625® plus alloy—A higher strength alternative to alloy 625, J Mater Eng Perform 1 (1992) 483–488. https://doi.org/10.1007/BF02682685.
28. ASTM International, ASTM G28-02: Standard Test Methods for Detecting Susceptibility to Intergranular Corrosion in Wrought, Nickel-Rich, Chromium-Bearing Alloys, (2015).
29. B. Rivolta, R. Gerosa, D. Panzeri, A. Nazim, Optimization of the Mechanical and Corrosion Resistance of Alloy 625 through Aging Treatments, Crystals (Basel) 14 (2024) 139. https://doi.org/10.3390/cryst14020139.
30. Carpenter Technology corporation, A guide to etching specialty alloys for microstructural evaluation, (2020). https://carpentertechnology.com/b log/a-guide-to-etching-specialty-alloys (accessed November 14, 2023).
31. BSI Standards, ISO 6507-1:2018: Metallic materials – Vickers hardness test, (2018).
32. BSI Standards Publication, BS EN ISO 6892-1:2019: Metallic materials - Tensile testing, (2020).
33. ASTM International, ASTM E112-13: Standard Test Methods for Determining Average Grain Size, (2013). https://doi.org/10.1520/E0112-13 (accessed August 23, 2023).